

Whole-exome sequencing identifies recessive *WDR62* mutations in severe brain malformations

Kaya Bilgüvar^{1,2,3*}, Ali Kemal Öztürk^{1,2,3*}, Angeliki Louvi^{1,2,3}, Kenneth Y. Kwan^{2,4}, Murim Choi³, Burak Tatlı⁵, Dilek Yalnızoğlu⁶, Beyhan Tüysüz⁷, Ahmet Okay Çağlayan⁸, Sarenur Gökben⁹, Hande Kaymakçalan¹⁰, Tanyeri Barak^{1,2,3}, Mehmet Bakırcıoğlu^{1,2,3}, Katsuhito Yasuno^{1,2,3}, Winson Ho^{1,2,3}, Stephan Sanders^{3,11,12}, Ying Zhu^{2,4}, Sanem Yılmaz⁹, Alp Dinçer¹³, Michele H. Johnson^{1,14,15}, Richard A. Bronen^{1,14}, Naci Koçer¹⁶, Hüseyin Per¹⁷, Shrikant Mane^{3,18}, Mehmet Necmettin Pamir¹⁹, Cengiz Yalçınkaya²⁰, Sefer Kumandaş¹⁷, Meral Topçu⁶, Meral Özmen⁵, Nenad Šestan^{2,4}, Richard P. Lifton^{3,21}, Matthew W. State^{3,11,12} & Murat Günel^{1,2,3}

The development of the human cerebral cortex is an orchestrated process involving the generation of neural progenitors in the periventricular germinal zones, cell proliferation characterized by symmetric and asymmetric mitoses, followed by migration of post-mitotic neurons to their final destinations in six highly ordered, functionally specialized layers^{1,2}. An understanding of the molecular mechanisms guiding these intricate processes is in its infancy, substantially driven by the discovery of rare mutations that cause malformations of cortical development^{3–6}. Mapping of disease loci in putative Mendelian forms of malformations of cortical development has been hindered by marked locus heterogeneity, small kindred sizes and diagnostic classifications that may not reflect molecular pathogenesis. Here we demonstrate the use of whole-exome sequencing to overcome these obstacles by identifying recessive mutations in *WD repeat domain 62 (WDR62)* as the cause of a wide spectrum of severe cerebral cortical malformations including microcephaly, pachygyria with cortical thickening as well as hypoplasia of the corpus callosum. Some patients with mutations in *WDR62* had evidence of additional abnormalities including lissencephaly, schizencephaly, polymicrogyria and, in one instance, cerebellar hypoplasia, all traits traditionally regarded as distinct entities. In mice and humans, *WDR62* transcripts and protein are enriched in neural progenitors within the ventricular and subventricular zones. Expression of *WDR62* in the neocortex is transient, spanning the period of embryonic neurogenesis. Unlike other known microcephaly genes, *WDR62* does not apparently associate with centrosomes and is predominantly nuclear in localization. These findings unify previously disparate aspects of cerebral cortical development and highlight the use of whole-exome sequencing to identify disease loci in settings in which traditional methods have proved challenging.

Malformations of cortical development are a diverse group of often devastating structural brain disorders reflecting deranged neuronal

proliferation, migration or organization. Application of traditional mapping approaches has proved to be particularly challenging for gene discovery in these syndromes, where kindreds with a single affected member are most common, linkage studies support high locus heterogeneity and recent genetic findings have fundamentally challenged previous diagnostic nosology^{3,7,8}. Based on the expectation that whole-exome sequencing using next generation platforms^{9–11} can markedly improve gene discovery efforts in these situations, we applied this technology to the index case of a small consanguineous kindred (NG 26) from eastern Turkey. The patient presented for medical attention owing to failure to reach developmental milestones and was found on clinical examination to have microcephaly. Neuroimaging studies identified a complex array of developmental abnormalities including pachygyria and thickened cortex (Figs 1a–d and 3c and Supplementary Videos 1 and 2).

We initially performed whole-genome genotyping of the two affected members to identify shared homozygous segments (each >2.5 centimorgans (cM)) that together composed 80.11 cM (Supplementary Table 1). Given the substantial length of these shared segments, we next performed whole-exome sequencing of the index case using Nimblegen solid-phase arrays and the Illumina Genome Analyser Iix instrument⁹. We achieved a mean coverage of 44X, and 94% of all targeted bases were read more than four times, sufficient to identify novel homozygous variants with high specificity (Supplementary Table 2). We identified two novel homozygous missense variants and one novel homozygous frameshift mutation within the shared homozygosity intervals (Supplementary Fig. 1 and Supplementary Table 3). The frameshift mutation occurred in *WDR62*, deleting four base pairs (bp) in exon 31 (Fig. 1e). The full-length *WDR62* (NM_001083961) maps to chromosome 19q13.12 and encodes 1,523 amino acids. The identified mutation causes a frameshift in codon 1,402, resulting in a premature stop codon at position 1,413 (Fig. 1f). The mutation was confirmed to be homozygous in both affected subjects and to be heterozygous in both

¹Department of Neurosurgery, Yale University School of Medicine, New Haven, Connecticut 06510, USA. ²Department of Neurobiology, Yale University School of Medicine, New Haven, Connecticut 06510, USA. ³Department of Genetics, Center for Human Genetics and Genomics and Program on Neurogenetics, Yale University School of Medicine, New Haven, Connecticut 06510, USA. ⁴Kavli Institute for Neuroscience, Yale University School of Medicine, New Haven, Connecticut 06510, USA. ⁵Division of Neurology, Department of Pediatrics, Istanbul University Istanbul Medical Faculty, Istanbul 34093, Turkey. ⁶Division of Neurology, Department of Pediatrics, Hacettepe University School of Medicine, Sıhhiye, Ankara 06100, Turkey. ⁷Division of Genetics, Department of Pediatrics, Istanbul University Cerrahpasa Faculty of Medicine, Istanbul 34098, Turkey. ⁸Department of Medical Genetics, Kayseri Education and Research Hospital, Kayseri 38010, Turkey. ⁹Division of Neurology, Department of Pediatrics, Ege University Faculty of Medicine, Izmir 35100, Turkey. ¹⁰Faculty of Arts and Sciences, Bahcesehir University, Istanbul 34353, Turkey. ¹¹Department of Psychiatry, Yale University School of Medicine, New Haven, Connecticut 06510, USA. ¹²Child Study Center, Yale University School of Medicine, New Haven, Connecticut 06510, USA. ¹³Department of Radiology, Acibadem University School of Medicine, Istanbul 34742, Turkey. ¹⁴Department of Radiology, Yale University School of Medicine, New Haven, Connecticut 06510, USA. ¹⁵Department of Otolaryngology, Yale University School of Medicine, New Haven, Connecticut 06510, USA. ¹⁶Department of Radiology, Istanbul University Cerrahpasa Faculty of Medicine, Istanbul 34098, Turkey. ¹⁷Division of Neurology, Department of Pediatrics, Erciyes University School of Medicine, Kayseri 38039, Turkey. ¹⁸Yale Center for Genome Analysis, Yale University School of Medicine, New Haven, Connecticut 06510, USA. ¹⁹Department of Neurosurgery, Acibadem University School of Medicine, Istanbul 34742, Turkey. ²⁰Division of Child Neurology, Department of Neurology, Istanbul University Cerrahpasa Faculty of Medicine, Istanbul 34098, Turkey. ²¹Howard Hughes Medical Institute, Yale University School of Medicine, New Haven, Connecticut 06510, USA.

*These authors contributed equally to this work.

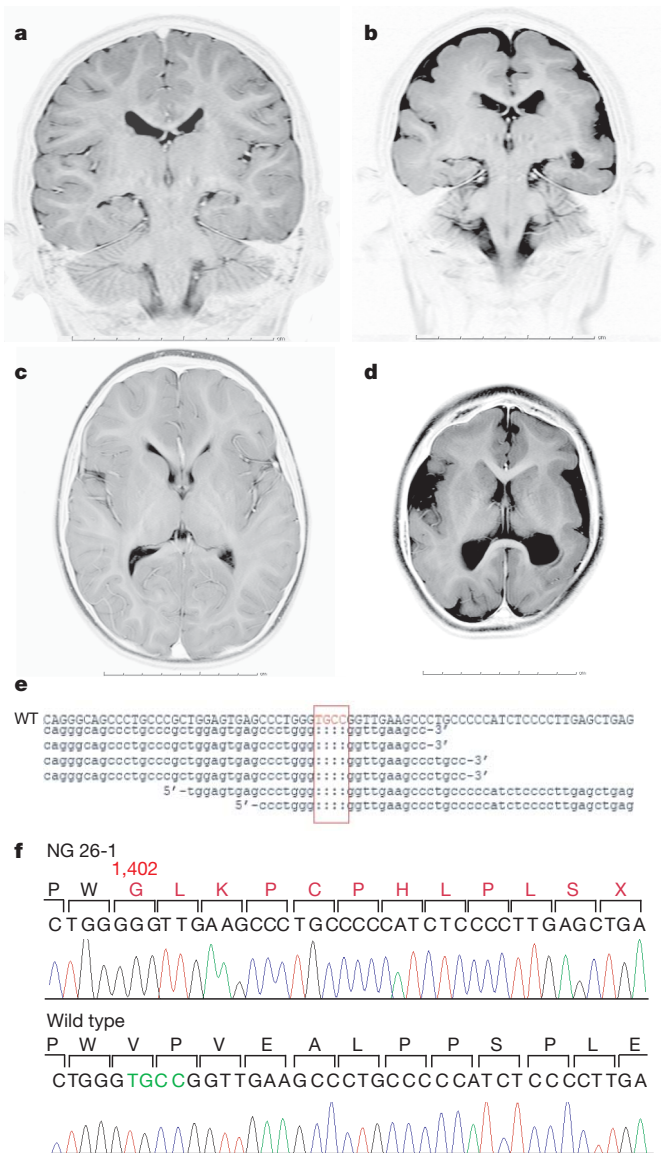


Figure 1 | Identification of a 4-bp deletion in the *WDR62* gene in a family with microcephaly and pachygyria. **a–d**, Coronal (**a**) and axial (**c**) magnetic resonance images of a control subject compared with NG 26-1 (**b**, **d**) confirms the clinical diagnosis of microcephaly and shows a diffusely thickened cortex, an indistinct grey–white junction, pachygyria and underopercularization. All images are T2 weighted (photographically inverted). Scale bars, centimetres. **e**, A 4-bp deletion (red box) in the *WDR62* is identified through exome sequencing (WT, wild type). **f**, Sanger sequencing confirms the deleted bases (in green). The altered amino-acid sequence (starting at position 1,402) leading to a premature stop-codon (X) is shown in red.

parents using Sanger sequencing (Fig. 2a and Supplementary Fig. 2). It was not observed in 1,290 Turkish control chromosomes.

Because this homozygous mutation in *WDR62* was particularly compelling, we sought to determine whether mutations in this gene might account for additional cases of malformations of cortical development. As the index case was ascertained with an initial diagnosis of pachygyria, we focused on a group of 30 probands who carried diagnoses of agyria or pachygyria and were products of consanguineous unions (inbreeding coefficient >1.5% (ref. 12)). Among these patients, whole-genome genotyping identified eight with homozygosity of at least 2 cM spanning the *WDR62* locus (Supplementary Information). One of these affected subjects, NG 891-1, was found to have the identical homozygous haplotype spanning the *WDR62* locus and had the same 4-bp deletion (Fig. 2a and Supplementary Fig. 2). Although there was no known relatedness between the two pedigrees,

the kinship coefficient of NG 891-1 with NG 26-1 (Fig. 2a, arrow) and NG 26-4 was 2.47% and 3.72%, consistent with fourth-degree relatedness (for example, first cousins once removed).

Further Sanger sequencing of the complete coding region of *WDR62* in the seven remaining kindreds revealed five additional novel homozygous mutations (Fig. 2b–f). The affected member of kindreds NG 30 and NG 294 had homozygous nonsense mutations at codons 526 (E526X) and 470 (Q470X), respectively (Fig. 2b, d); subject NG 339-1 had a homozygous 17-bp deletion leading to a frameshift at codon 1,280 that resulted in a premature termination codon following a novel peptide of 20 amino acids (Fig. 2e); subjects NG 190-1 and NG 537-1 respectively had novel homozygous missense variants W224S and E526K (Fig. 2c, f), which occurred at positions highly conserved among vertebrates and were predicted to be deleterious by the Polyphen algorithm (Supplementary Fig. 3). Moreover, after identification of the W224S mutation in NG 190, we ascertained two additional relatives affected with microcephaly and mental retardation (kinship coefficients of 4.47% and 5.81%) both of whom also proved to be homozygous for the same mutation. The resulting lod score for linkage to the trait within the expanded kindred was 3.64; the chromosome segment containing *WDR62* was the sole homozygous region shared among all three affected subjects (Supplementary Fig. 4).

All of the newly identified mutations, except E526K, were absent from 1,290 Turkish and 1,500 caucasian control chromosomes. The heterozygous E526K variant was detected in three apparently unrelated Turkish individuals who were neurologically normal (allele frequency 0.2%). As an additional control measure in the evaluation of these homozygous mutations, we sequenced the coding region of the gene in 12 consanguineous patients with non-neurological conditions who were found to have segments of homozygosity of at least one million base pairs spanning *WDR62*. None of these 12 individuals had protein coding changes in *WDR62* (data not shown). Similarly, we identified only four heterozygous novel missense variants in *WDR62* in the sequence of 100 whole exomes of subjects with non-neurological diseases (Supplementary Table 4). Public databases (dbSNP) showed no validated nonsense or frameshift alleles at this locus. Finally, we have not observed any copy number variants overlapping the coding regions of *WDR62* in our own set of 11,320 whole-genome genotypes (data not shown) and only one deletion identified by bacterial artificial chromosome (BAC) array is reported in the Database of Genomic Variants (<http://projects.tcag.ca/variation/>).

All of the index cases with *WDR62* mutations presented for medical attention with mental retardation and were found to have prominent microcephaly on physical examination; some also suffered from seizures (Supplementary Information). Re-examination of the high field strength (3 T) magnetic resonance imaging (MRI) scans of the affected subjects by independent neuroradiologists who were blind to previous diagnoses identified hallmarks of a wide range of severe cortical malformations (summarized in Supplementary Table 5 and shown in Supplementary Videos). All nine patients had extreme microcephaly, pachygyria and hypoplasia of the corpus callosum (Fig. 3). In addition, they demonstrated radiographic features consistent with lissencephaly, including varying degrees of cortical thickening and loss of grey–white junction (Fig. 3). Under-opercularization (shallow Sylvian fissures) (Fig. 1b) was observed in six affected subjects. Two of the subjects had striking polymicrogyria that predominantly affected one hemisphere (Fig. 3c, d, g); in one this was associated with a unilateral open-lip schizencephaly characterized by a cleft surrounded by grey matter that extended into the ventricle (Fig. 3d, g). Other malformations observed included hippocampal dysmorphology with vertical orientation in six cases and a single case of unilateral dysgenesis of the cerebellum (Fig. 3f). There were no abnormalities of the brainstem, with the exception of unilateral atrophy observed in one patient, most likely secondary to Wallerian degeneration from the severe cerebral abnormalities observed (Fig. 3h).

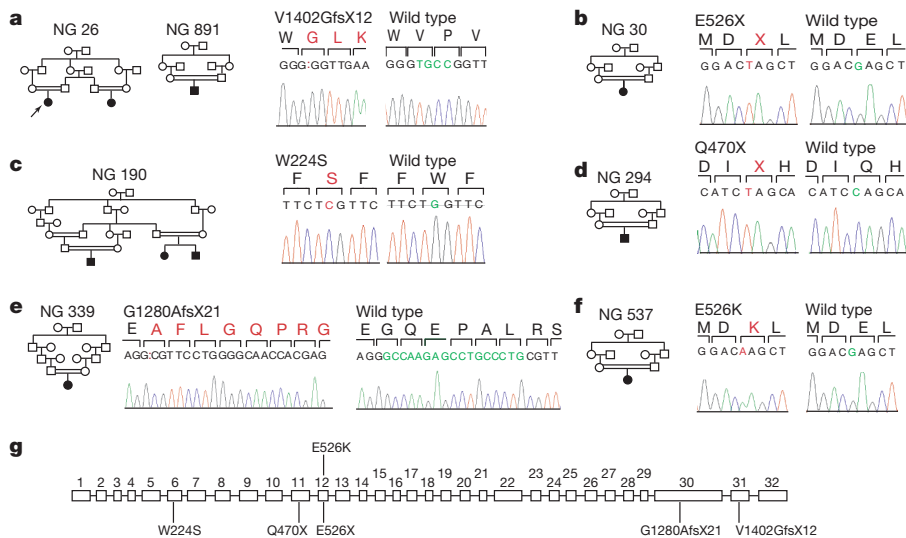


Figure 2 | Additional WDR62 mutations. **a–f**, Pedigree structures with mutated bases (red) and the corresponding normal alleles (green) are marked on the chromatograms (left, mutant; right, wild type). **a**, Families NG 26 and NG 891 harbour the identical 4-bp deletion, whereas nonsense mutations leading to premature stop codons (X) are observed in NG 30 (**b**) and NG 294 (**d**). Missense mutations affecting conserved amino acids are seen in NG 190 (**c**) and NG 537 (**f**). In NG 339 (**e**), a 17-bp deletion leads to a premature stop codon. **g**, The locations of independent mutations are indicated on the genomic organization of WDR62.

Given the wide range of cortical malformations associated with WDR62 mutations, we next investigated its expression in the developing mouse brain. Notably, during early development, in wholemount embryos from embryonic day (E) 9.5 to E11.5, Wdr62 expression is prominent in neural crest lineages (Supplementary Fig. 5a–c). Wdr62 also shows striking expression in the ventricular and subventricular zones during the period of cerebral cortical neurogenesis (E11.5–16.5), with expression decreasing in intensity by E17.5 (Fig. 4a, Supplementary Fig. 5d–f and data not shown). In the cerebellum, Wdr62 is strongly expressed in precursors of granule neurons at late embryonic and early postnatal stages; by postnatal day 9 (P9) Wdr62

expression is dramatically reduced (Supplementary Fig. 5g, h). By postnatal day 21 (P21), low levels of Wdr62 expression are detected only in the hippocampus and the piriform cortex, and transcription is absent among differentiated cortical neurons (Supplementary Fig. 5i).

We next examined WDR62 protein expression using a previously characterized antibody¹³ (Fig. 4b–d). Both in the mouse and human fetal brain, WDR62 was enriched within the ventricular and subventricular

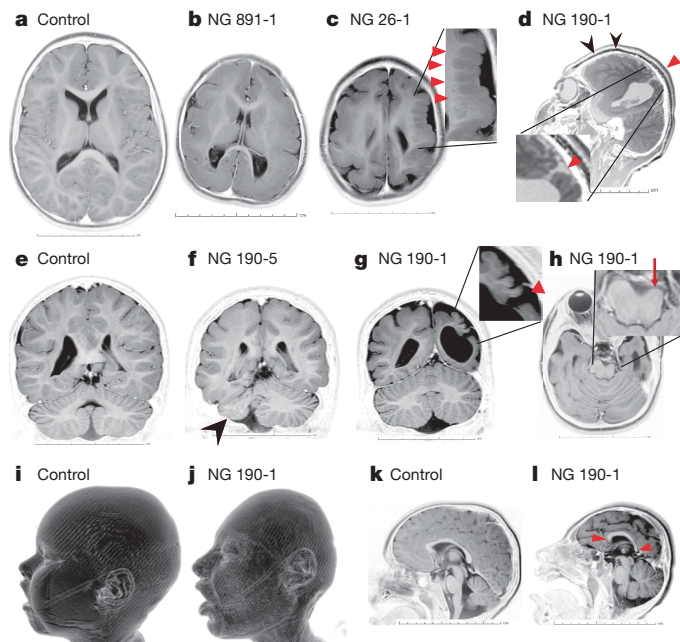


Figure 3 | Representative magnetic resonance images from patients demonstrating the wide spectrum of findings associated with mutations in WDR62. **a, e, i, k**, Axial (**a**), coronal (**e**), sagittal (**k**) MRI images and three-dimensional surface rendering (**i**) of a control subject are shown. **b**, Microlissencephalic features with microcephaly, diffusely thickened cortex, loss of grey–white junction and pachygyria. **c**, Asymmetric microcephalic hemispheres with marked polymicrogyria (arrowheads). **d**, Significant polymicrogyria (black arrowheads) and open-lip schizencephaly (red arrowhead). **f**, Unilateral cerebellar hypoplasia (arrowhead). **g**, Open-lip schizencephaly (red arrowhead) and the polymicrogyric cortex. **h**, Unilateral brainstem atrophy (arrow). **j**, Three-dimensional surface rendering demonstrating craniofacial dysmorphism. **l**, Microcephaly, pachygyria and abnormally shaped corpus callosum (arrowheads).

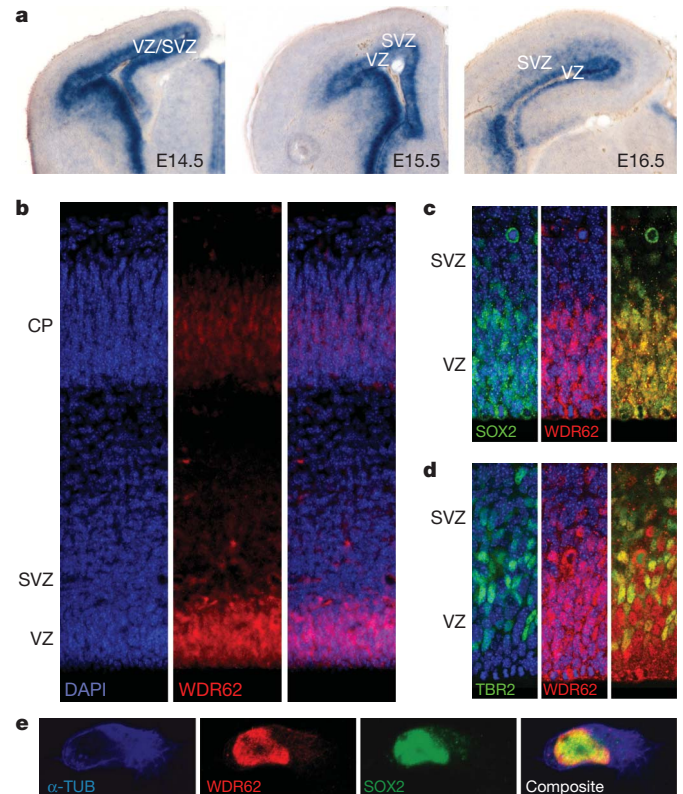


Figure 4 | Wdr62 expression in the developing mouse brain. **a**, Wdr62 expression is enriched in the ventricular and subventricular zones (VZ and SVZ, respectively) as seen with *in situ* hybridization. **b**, WDR62 protein (red) distribution reveals a similar pattern. CP, cortical plate. **c, d**, WDR62 (red) localizes to the nuclei and is expressed by neural stem cells and intermediate progenitors, as marked by SOX2 and TBR2 expression (green), respectively. **e**, Immunofluorescence staining for α-tubulin (cytoplasmic, blue), SOX2 (nuclear, green) and WDR62 (red) in E12.5 cortical neural progenitor cells reveals that the distribution of the WDR62 overlaps with that of SOX2 and is predominantly nuclear. (Nuclear staining by 4',6-diamidino-2-phenylindole (DAPI) (blue) in **b–d**; rightmost panels are composite images in **b–e**).

zones, consistent with our *in situ* hybridization findings (Fig. 4 and Supplementary Fig. 6). These stainings suggested that WDR62 localizes predominantly to the nucleus in neuronal cells, which we confirmed by immunofluorescence microscopy using cell cultures and western blotting with subcellular fractionation of cortical embryonic mouse cells with a second antibody (Fig. 4e and Supplementary Fig. 7). Genes previously implicated in microcephaly encode centrosomal proteins^{14–16}; thus it is noteworthy that WDR62 is apparently not associated with the centrosome during mitosis (Supplementary Fig. 8).

Our findings implicate WDR62 in the pathogenesis of a spectrum of cortical abnormalities that until now have largely been conceptualized to be distinct^{3,7,8}, suggesting that these diverse features can have unified underlying causation. It is noteworthy that WDR62 lies in a 10-million-bp interval that had previously been identified as a microcephaly locus, *MCPH2* (ref. 17). Although there were no imaging studies presented in the previous mapping of this locus, our findings suggest that WDR62 is the *MCPH2* gene and extend the phenotype beyond microcephaly.

To seek further insight into the biological function of WDR62, we examined expression data of early embryonic development of mouse brain (GSE8091)¹⁸ for genes with expression profiles significantly correlated with that of WDR62 (Bonferroni corrected $P < 0.01$, $n = 1,104$). Functional annotation suggested that positively correlated genes were enriched for those encoding nuclear proteins (Benjamini adjusted $P = 6.23 \times 10^{-30}$), RNA processing proteins (Benjamini adjusted $P = 1.90 \times 10^{-31}$) and cell-cycle proteins (Benjamini adjusted $P = 3.25 \times 10^{-18}$). Negatively correlated genes encoded neuronal differentiation proteins (Benjamini adjusted $P = 1.40 \times 10^{-7}$). Several genes linked to developmental brain malformations, such as *DCX*, *DCC* and *BURB1B*, are found in these enrichment sets (Supplementary Table 6). Further work will be required to extend these expression findings and clarify the normal role of WDR62.

So far, whole-exome sequencing has led to the identification of a single new Mendelian locus for a genetically homogeneous condition¹⁰. Our results demonstrate that this technology will be particularly valuable for gene discovery in those conditions in which mapping has been confounded by locus heterogeneity and uncertainty about the boundaries of diagnostic classification, pointing to a bright future for its broad application to medicine.

METHODS SUMMARY

Human subjects. The study protocol was approved by the Yale Human Investigation Committee. Approvals from institutional review boards for genetic studies, and written consent from all study subjects, were obtained at the participating institutions (Supplementary Information).

Targeted exome sequencing. Genomic DNA of sample NG 26-1 was captured on a NimbleGen 2.1M Human Exome Array with modifications to the manufacturer's protocol⁹, followed by single-read cluster generation on the Cluster Station (Illumina). The captured, purified and clonally amplified library targeting the exome from patient NG 26-1 was then sequenced on Genome Analyser IIX. Two lanes of single-read sequencing at a read length of 74 bp was performed following the manufacturer's protocol.

Exome sequence analysis. The sequence reads obtained were aligned to the human genome (hg18) using Maq¹⁹ and BWA²⁰ software. The percentage alignment of the reads to both the reference genome as well as the targeted region, exome, was calculated using Perl scripts⁹. Similarly, Perl scripts were used for the detection of mismatch frequencies and error positions. SAMtools²¹ was used for the detection of single-nucleotide variations on the reads aligned with Maq. The indels were detected on the reads aligned with BWA for its ability to allow for gaps during the alignment. Shared homozygous segments of the affected individuals were detected using Plink software version 1.06 (ref. 12), and the variants were filtered for shared homozygosity. The variants were annotated for novelty compared with both dbSNP (build 130) and nine personal genome databases and previous exome sequencing experiments performed by our human genomics group. Novel variants were further evaluated for their impact on the encoded protein, conservation across 44 vertebrate species, *Caenorhabditis elegans* and *Drosophila melanogaster*, expression patterns and potential overlap with known microRNAs.

Full Methods and any associated references are available in the online version of the paper at www.nature.com/nature.

Received 11 May; accepted 30 June 2010.

Published online 22 August 2010.

- Bystron, I., Blakemore, C. & Rakic, P. Development of the human cerebral cortex: Boulder Committee revisited. *Nature Rev. Neurosci.* **9**, 110–122 (2008).
- Rakic, P. Evolution of the neocortex: a perspective from developmental biology. *Nature Rev. Neurosci.* **10**, 724–735 (2009).
- Guerrini, R., Dobyns, W. B. & Barkovich, A. J. Abnormal development of the human cerebral cortex: genetics, functional consequences and treatment options. *Trends Neurosci.* **31**, 154–162 (2008).
- Guerrini, R. Genetic malformations of the cerebral cortex and epilepsy. *Epilepsia* **46** (suppl. 1), 32–37 (2005).
- Guerrini, R. & Carrozzo, R. Epilepsy and genetic malformations of the cerebral cortex. *Am. J. Med. Genet.* **106**, 160–173 (2001).
- Mochida, G. H. & Walsh, C. A. Molecular genetics of human microcephaly. *Curr. Opin. Neurol.* **14**, 151–156 (2001).
- Barkovich, A. J., Kuzniecky, R. I., Jackson, G. D., Guerrini, R. & Dobyns, W. B. Classification system for malformations of cortical development: update 2001. *Neurology* **57**, 2168–2178 (2001).
- Barkovich, A. J., Kuzniecky, R. I., Jackson, G. D., Guerrini, R. & Dobyns, W. B. A developmental and genetic classification for malformations of cortical development. *Neurology* **65**, 1873–1887 (2005).
- Choi, M. et al. Genetic diagnosis by whole exome capture and massively parallel DNA sequencing. *Proc. Natl Acad. Sci. USA* **106**, 19096–19101 (2009).
- Ng, S. B. et al. Exome sequencing identifies the cause of a mendelian disorder. *Nature Genet.* **42**, 30–35 (2010).
- Ng, S. B. et al. Targeted capture and massively parallel sequencing of 12 human exomes. *Nature* **461**, 272–276 (2009).
- Purcell, S. et al. PLINK: a tool set for whole-genome association and population-based linkage analyses. *Am. J. Hum. Genet.* **81**, 559–575 (2007).
- Wasserman, T. et al. A novel c-Jun N-terminal kinase (JNK)-binding protein WDR62 is recruited to stress granules and mediates a nonclassical JNK activation. *Mol. Biol. Cell* **21**, 117–130 (2010).
- Bond, J. et al. A centrosomal mechanism involving CDK5RAP2 and CENPJ controls brain size. *Nature Genet.* **37**, 353–355 (2005).
- Kumar, A., Girimaji, S. C., Duvvari, M. R. & Blanton, S. H. Mutations in STIL, encoding a pericentriolar and centrosomal protein, cause primary microcephaly. *Am. J. Hum. Genet.* **84**, 286–290 (2009).
- Thornton, G. K. & Woods, C. G. Primary microcephaly: do all roads lead to Rome? *Trends Genet.* **25**, 501–510 (2009).
- Roberts, E. et al. The second locus for autosomal recessive primary microcephaly (*MCPH2*) maps to chromosome 19q13.1–13.2. *Eur. J. Hum. Genet.* **7**, 815–820 (1999).
- Hartl, D. et al. Transcriptome and proteome analysis of early embryonic mouse brain development. *Proteomics* **8**, 1257–1265 (2008).
- Li, H., Ruan, J. & Durbin, R. Mapping short DNA sequencing reads and calling variants using mapping quality scores. *Genome Res.* **18**, 1851–1858 (2008).
- Li, H. & Durbin, R. Fast and accurate short read alignment with Burrows-Wheeler transform. *Bioinformatics* **25**, 1754–1760 (2009).
- Li, H. et al. The Sequence Alignment/Map format and SAMtools. *Bioinformatics* **25**, 2078–2079 (2009).

Supplementary Information is linked to the online version of the paper at www.nature.com/nature.

Acknowledgements We are indebted to the patients and families who have contributed to this study. We thank J. Noonan for expert advice and C. Computaro for her help with three-dimensional reconstruction of the magnetic resonance images. This study was supported by the Yale Program on Neurogenetics, the Yale Center for Human Genetics and Genomics, and National Institutes of Health grants RC2 NS070477 (to M.G.), UL1 RR024139NIH (Yale Clinical and Translational Science Award) and UO1MH081896 (to N.S.). SNP genotyping was supported in part by a National Institutes of Health Neuroscience Microarray Consortium award U24 NS051869-02S1 (to S.M.). R.P.L. is an investigator of the Howard Hughes Medical Institute.

Author Contributions M.W.S., R.P.L. and M.G. designed the study and K.B., A.L., N.S., R.P.L. and M.G. designed the experiments. K.B., A.K.O., A.L., K.Y.K., T.B., M.B., S.S., W.H. and S.M. performed the experiments. B.T., D.Y., B.T., A.O.C., S.G., H.K., S.Y., H.P., C.Y., S.K., M.T. and M.O. identified, consented and recruited the study subjects and provided clinical information. A.D., M.H.J., R.A.B., N.K. and M.N.P. performed and evaluated magnetic resonance imaging. M.C. and R.P.L. developed the bioinformatics scripts for data analysis. K.B., A.K.O., K.Y., A.L. and M.G. analysed the genetics data. A.L., K.Y.K., Y.Z., N.S. and M.G. analysed the expression data. K.B., A.K.O., A.L., R.P.L., M.W.S. and M.G. wrote the paper.

Author Information Reprints and permissions information is available at www.nature.com/reprints. The authors declare competing financial interests: details accompany the full-text HTML version of the paper at www.nature.com/nature. Readers are welcome to comment on the online version of this article at www.nature.com/nature. Correspondence and requests for materials should be addressed to R.P.L. (richard.lifton@yale.edu), M.W.S. (matthew.state@yale.edu) or M.G. (murat.gunel@yale.edu).

METHODS

Human subjects. The study protocol was approved by the Yale Human Investigation Committee. Approvals from institutional review boards for genetic studies, and written consent from all study subjects, were obtained at the participating institutions (Supplementary Information).

MRI sequences. MRI examinations presented were performed with a 3-T scanner (Trio, Siemens).

Illumina genotyping. Whole-genome genotyping of the samples was performed on the Illumina Platform with Illumina Human 370K Duo or 610K Quad Beadchips using the manufacturer's protocol. The image data were normalized and the genotypes were called using data analysis software (Bead Studio, Illumina). Linkage analysis was performed using Allegro version 2.0 software (DeCode Genetics).

Sanger sequencing. The exons and exon–intron boundaries of *WDR62* were determined using the University of California, Santa Cruz (UCSC) Genome Browser (<http://genome.ucsc.edu>); unique primers were designed using Sequencher 4.8 (Gene Codes) and synthesized by Invitrogen. The fragments were amplified, purified and direct re-sequencing was performed using ABI's 9800 Fast Thermocyclers. The amplicons were analysed on an 3730xL DNA Analyser (Applied Biosystems).

Targeted sequence capture. Genomic DNA of sample NG 26-1 was captured on a NimbleGen 2.1M Human Exome Array (based on the build of 30 April 2008 of the consensus coding sequence (CCDS) database) with modifications to the manufacturer's protocol⁹. The pre- and post-capture libraries were compared by quantitative PCR for the determination of the relative fold enrichment of the targeted sequences.

Exome sequencing. Single-read cluster generation was performed on the Cluster Station (Illumina). The captured, purified and clonally amplified library targeting the exome from patient NG 26-1 was sequenced on Genome Analyser IIx. Two lanes of single-read sequencing at a read length of 74 bp was performed following the manufacturer's protocol. Image analysis and base calling was performed by Illumina Pipeline version 1.5 with default parameters, installed on Yale University's High Performance Computing Cluster.

Exome sequence analysis. The sequence reads obtained were aligned to the human genome (hg18) using Maq¹⁹ and BWA²⁰ software. The percentage alignment of the reads to both the reference genome as well as the targeted region, exome, was calculated using perl scripts⁹. Similarly, perl scripts were used for the detection of mismatch frequencies and error positions. SAMtools²¹ was used for the detection of single-nucleotide variations on the reads aligned with Maq. The indels were detected on the reads aligned with BWA for its ability to allow for gaps during the alignment. Shared homozygous segments of the affected individuals were detected using PLINK software version 1.06 (ref. 12), and the variants were filtered for shared homozygosity. The variants were annotated for novelty compared with both dbSNP (build 130) and nine personal genome databases and previous exome sequencing experiments performed by our human genomics groups.

Functional annotation. Published microarray data sets of E9.5, E11.5 and E13.5 mouse brain tissue (GSE8091) were downloaded from the GEO database (<http://www.ncbi.nlm.nih.gov/projects/geo/query/acc.cgi>)¹⁸ and processed using R statistical program (Affy package)²². Genes that correlated highly with *Wdr62* (Bonferroni corrected $P < 0.01$) were functionally annotated using DAVID tools (<http://david.abcc.ncifcrf.gov/>)²³.

Animals. Experiments were performed in accordance with protocols approved by the Institutional Animal Care and Use Committee at Yale University School of Medicine.

In situ hybridization. Sections and wholemount embryos were processed for non-radioactive *in situ* hybridization as described previously with minor modifications²⁴. An RNA probe complementary to mouse *Wdr62* (bases 3,525–4,480

of the mouse *Wdr62* complementary DNA, NM_146186) was prepared and labelled with digoxigenin-11-uridine-5'-triphosphate. Embryos and tissue sections were analysed using a Zeiss Stemi dissecting microscope or a Zeiss AxioImager fitted with a Zeiss AxioCam MRc5 digital camera. Images were captured using AxioVision AC software (Zeiss) and assembled using Adobe Photoshop.

Immunostaining and confocal imaging. E15.5 embryos were obtained from timed-pregnant CD-1 mice (Charles River). For timed pregnancies, midday of the day of vaginal plug discovery was considered E0.5. Dissected brains were fixed by immersion in 4% paraformaldehyde for 16 h at 4 °C and sectioned at 70 µm using a vibratome (Leica VT1000S). Human fetal brains at 19 and 20 weeks' gestation were obtained under the guidelines approved by the Yale Institutional Review Board (protocol number 0605001466) from the Human Fetal Tissue Repository at the Albert Einstein College of Medicine (CCI number 1993-042), fixed by immersion in 4% paraformaldehyde for 36 h, cryoprotected and frozen, and cryosectioned at 60 µm. For mouse sections, an unconjugated donkey anti-mouse IgG Fab fragment (Jackson Immuno Research Laboratories, 1:200) was added to block endogenous mouse IgG. Primary antibodies were diluted in blocking solution at the following dilutions: mouse anti-WDR62 (Sigma-Aldrich), 1:400; rabbit anti-SOX2 (Millipore), 1:500; rabbit anti-TBR2 (Abcam), 1:500; chicken anti-GFP (Abcam), 1: 1,500; rat anti- α -tubulin (Abcam), 1:500; rabbit anti- γ -tubulin (Sigma), 1:250; standard methods were followed. Confocal images were collected using laser-scanning microscope (Zeiss LSM 510). For diaminobenzidine staining, brain sections were incubated with biotinylated secondary antibodies and processed using the ABC and diaminobenzidine kits (Vector Laboratories). Images were acquired using a digital scanner (Aperio).

Cell culture. For neural progenitor cultures, dorsal telencephalon was dissected from E12.5 mouse embryos and enzymatically dissociated and re-suspended as previously described²⁵. For cell lines, Neuro2a, HeLa and HEK-293FT cells were plated on glass coverslips coated with poly-L-ornithine (15 µg ml⁻¹) at 5 × 10⁵ cells per square centimetre in 24-well plates. Sixteen hours after plating, the cells were fixed by immersion in 4% paraformaldehyde for 15 min at room temperature and processed for immunostaining.

Subcellular fractionation and western blotting. Dorsal telencephalon was dissected from E14.5 mouse embryos and fractionated using the CellLytic nuclear extraction kit (Sigma). The manufacturer's protocol was followed with the exception that cell lysis was achieved by addition of 0.5% Triton X-100. Immunoblotting was done with primary antibodies at the following dilutions: rabbit anti-WDR62 (Novus), 1:1,000; rat anti- α -tubulin (Abcam), 1:5,000.

In utero electroporation. CAG–GFP plasmid DNA was transfected into ventricular zone progenitors of E13.5 embryos by *in utero* electroporation as previously described²⁶. At E15.5, the embryos were collected and fixed for immunostaining.

22. Irizarry, R. A. *et al.* Summaries of Affymetrix GeneChip probe level data. *Nucleic Acids Res.* **31**, e15 (2003).
23. Huang da, W., Sherman, B. T. & Lempicki, R. A. Systematic and integrative analysis of large gene lists using DAVID bioinformatics resources. *Nature Protocols* **4**, 44–57 (2009).
24. Stillman, A. A. *et al.* Developmentally regulated and evolutionarily conserved expression of SLITRK1 in brain circuits implicated in Tourette syndrome. *J. Comp. Neurol.* **513**, 21–37 (2009).
25. Abelson, J. F. *et al.* Sequence variants in SLITRK1 are associated with Tourette's syndrome. *Science* **310**, 317–320 (2005).
26. Kwan, K. Y. *et al.* SOX5 postmitotically regulates migration, postmigratory differentiation, and projections of subplate and deep-layer neocortical neurons. *Proc. Natl Acad. Sci. USA* **105**, 16021–16026 (2008).

Supplementary Notes

Clinical Histories of Patients with *WDR62* Mutations

This study was approved by the Yale Human Investigation Committee (9406007680 (10/24/2009) and 0908005592 (8/17/2009)). Consents were obtained from all study participants by the referring physicians. IRB protocol numbers and approval dates are as follows: Istanbul: NO:C-033 (12/22/2009); Hacettepe: 2008ABH67540017 (9/27/2007); Kayseri: 2009/55 (9/3/2009); Ege: B.30.2.EGE.0.20.05.00/OM/1093-1432, #09-5.1/16, (6/23/2009).

NG 26-1 (mutation: V1402GfsX12):

The patient is a 4 year 6 month old female who was the product of a consanguineous union. She was brought to medical attention at 4 months of age due to small head size. At that time, her head circumference was 33 cm and she was given a diagnosis of microcephaly. Metabolic and TORCH workups were negative. She was last seen in clinic at 2 years and 3 months of age. Her head circumference was 38 cm. She showed micrognathia and a bulbous nose, and suffered from severe mental retardation. She was able to say a few words including "cat", "dad", "come", and "new", and responded to basic verbal commands. She was not toilet trained nor able to feed herself. She was able to walk and run, but could not ascend or descend stairs. Her vision and hearing were noted to be unremarkable. She has no spasticity in any of her extremities and has never experienced any seizures.

NG 30-1 (mutation: E526X):

The patient is a 7-year-old female who is the product of a consanguineous union. The pregnancy was uneventful and the neonatal period was unremarkable. The patient presented to medical attention at 9 months of age due to small head size. On examination, she was found to have motor retardation. Her head circumference at that time was noted to be 38.5 cm and she was diagnosed with microcephaly. She had an unrevealing metabolic workup. At the age of 4, she began experiencing generalized seizures which were controlled with levetiracetam. Her last clinic visit was at the age of 6. At that visit, she was able to ambulate independently, was able to understand only basic verbal commands, had limited vocabulary, and was noted to have moderate mental retardation based on clinical examination.

NG 190-1 (mutation: W224S):

The patient is a 6 year 5 month old boy who is the product of a consanguineous union. His peri- and neonatal periods were unremarkable. He presented to medical attention at the age of 2 due to hyperactivity, seizures, and inability to sleep. The seizures were generalized, tonic/clonic, lasting approximately 1-2 minutes each and occurring on average twice a day. At that time on neurologic exam, he was able to speak 1-2 word sentences. Motor tone and bulk were grossly normal. Reflexes were within normal limits and cranial nerves were intact. At the most recent clinic visit in 2009, he continued to experience 4-8 seizures per day and was being treated with valproic acid. Physical exam revealed microcephaly and micrognathia. His head circumference was noted to be 42 cm and he had severe mental retardation based on clinical observation. He was not toilet trained, could only speak a single word, "dad", could not feed himself, and was only able to ambulate with the support of others.

NG 190-5 (mutation: W224S):

This patient is an 8 year 7 month old female who is the product of a consanguineous marriage and the cousin of NG 190-1. The patient presented to medical attention at the age of 3 due to seizures. She is microcephalic, hyperactive, and has dysconjugate gaze. On the most recent exam her head circumference was 44 cm and she was noted to have moderate mental retardation based on clinical observation. She demonstrated poor verbal skills, but was able to carry out simple activities of daily living. She had normal tone, reflexes, and no dysmetria on exam. She was able to walk independently, and had no obvious dysmorphic features. She was grossly less affected than her brother (NG 190-6) and cousin (NG 190-1).

NG 190-6 (mutation: W224S):

This patient is a 12 year, 11 month old boy who is the product of a consanguineous marriage and is the brother of patient NG 190-5. He has a history of seizures and mental and motor retardation. He is noted to have microcephaly (current head circumference is 45 cm) and self-mutilating behaviors. On last exam, his gaze was described as dysconjugate, muscle tone was increased, and reflexes were hyperactive. He was assessed as having severe mental retardation based on clinical exam, but could ambulate independently. His symptoms are notably more severe than his sister's.

NG 294-1 (mutation: Q470X):

The patient is a 14 year, 6 month old male who is the product of a consanguineous marriage. He has two normal siblings. His perinatal history is significant for preterm birth at 32 weeks of gestation. He was hospitalized at 27 days for bilirubinemia at which time he was found to have genu varum (bow leggedness) and microcephaly. He has had two deformity correction surgeries since that time, a hernia repair at 2 months, and cryptorchidism repair at 8 years of age. He has celiac disease, arachnodactyly, microcephaly and severe mental retardation diagnosed by clinical observation. He has never suffered a seizure.

NG 339-1 (mutation: G1280AfsX21):

The patient is a 10 year, 10 month old female who is the product of a consanguineous union. She presented to medical attention at 3 months of age due to failure to thrive and small head size. At the time of presentation her head circumference was 34.5 cm with obvious microcephaly. On neurologic examination, she had good head control. She recognized her mother and was noted to have a social smile. Her deep tendon reflexes (DTR's) were 3+ in all four extremities and she had increased muscle tone throughout. She has one healthy sibling. No current clinical information is available.

NG 537-1 (mutation: E526K):

The patient is a 15 year, 5 month old female who is the product of consanguineous marriage. Peri- and neonatal periods were unremarkable except for meconium aspiration. She was delayed to acquire motor skills in the first three years of life but ultimately presented to medical attention at the age of 3.5 years due to poor verbal skills. Head circumference at this time was 43 cm, consistent with microcephaly. She was noted to have severe mental retardation, but the remainder of the neurologic exam at the time was normal. She was placed on anti-epileptic medication for a brief period of time during her childhood due to abnormal electroencephalograms (EEG's), however, she never suffered an overt seizure. The medication was discontinued. At her last clinic visit in 2009, her head circumference was 51 cm. On physical exam, she was noted to have microcephaly, prognathism, dysconjugate gaze, and dysarthria. She was able to ambulate independently, demonstrated full strength in all muscle groups, and had normal reflexes.

NG 891-1 (mutation: V1402GfsX12):

The patient is a 2 year 4 month old male who was born to consanguineous parents. He had a normal prenatal and neonatal period and was the product of an uneventful vaginal delivery. He presented to medical attention at 20 months of age due to relatively small head size compared to his healthy sibling. At the time of presentation, he was 9,500 gr (50-75th percentile) and 83 cm (50th percentile). His head circumference, however, was 41 cm (<3 percentile). He was noted on clinical exam to have developmental delay and severe psychomotor retardation but has not suffered from seizures.

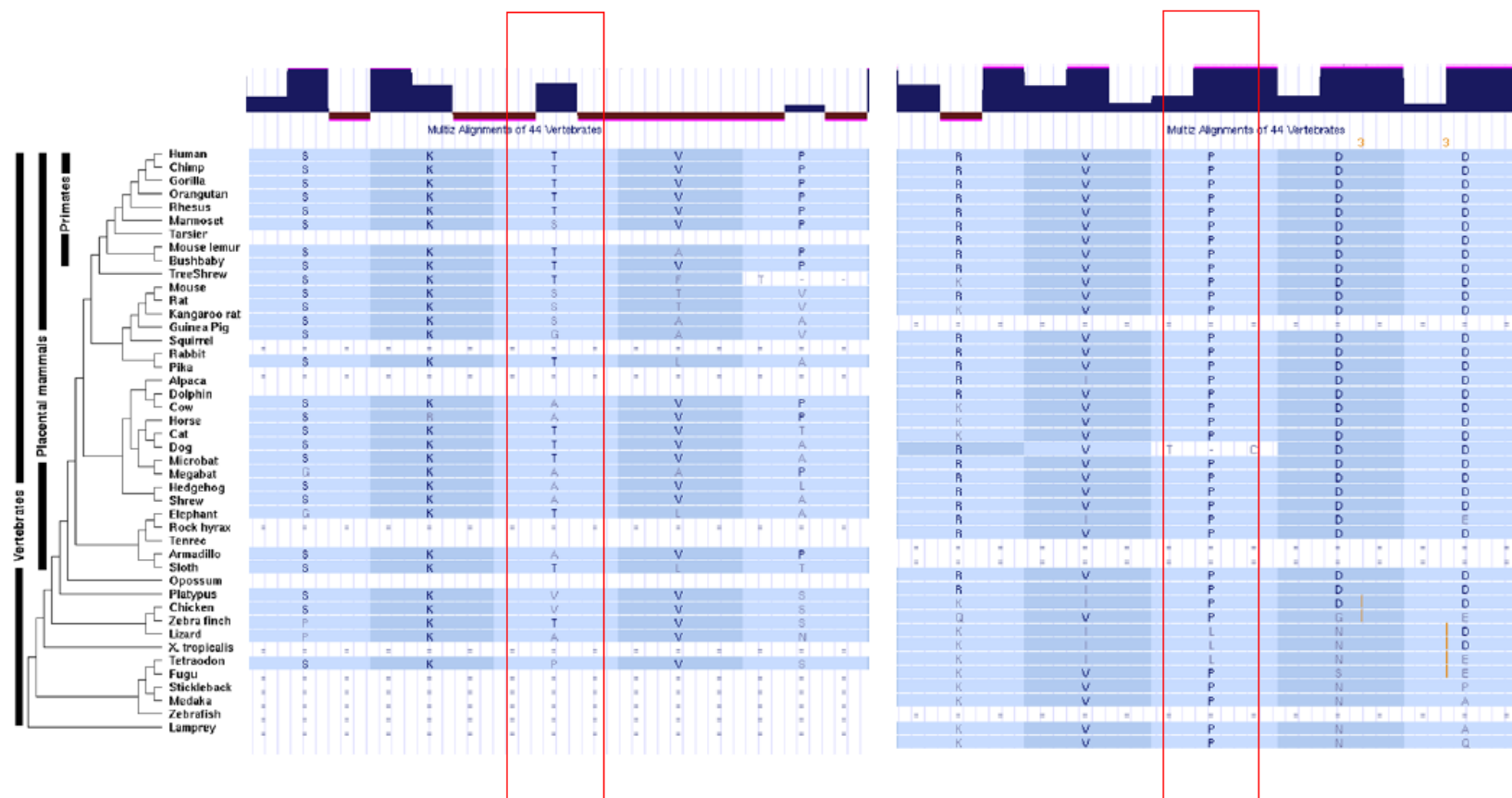
Supplementary Videos

Supplementary Videos 1 and 2, Videos constructed from T2 sagittal (Supplementary Video 1) and coronal (Supplementary Video 2) images (photographically inverted) of patient NG 26-1 demonstrate microcephaly and cortical thickening. The gray-white junction is ill-defined, and there is a deep sulcus in the right parieto-occipital lobe. There is diffuse pachgyria, mainly affecting the left hemisphere. Note the simplification of the gyral-sulcal pattern, underopercularization and the overall decreased brain volume. The brainstem and cerebellum are grossly normal.

Supplementary Videos 3 and 4, Videos constructed from T2 sagittal (Supplementary Video 3) and coronal (Supplementary Video 4) images of patient NG 190-1 (photographically inverted) shows diffuse cortical volume loss and marked craniofacial disproportion. There is diffuse polymicrogyria, most visible in the left posterior frontal lobe associated with a schizencephalic cleft lined with gray matter suggesting that this is a developmental process and not due to *in utero* problems, which typically lead to porencephalic cysts lined with white matter. In addition, cortical thickening, most prominent in the bilateral frontal lobes can be appreciated. Hemiatrophy of the left hemisphere with resultant *ex vacuo* enlargement of the ipsilateral ventricle is seen. Hypoplasia of the corpus callosum is best visible on the midline sagittal images. In addition, atrophy of the left side of the brain stem is seen.

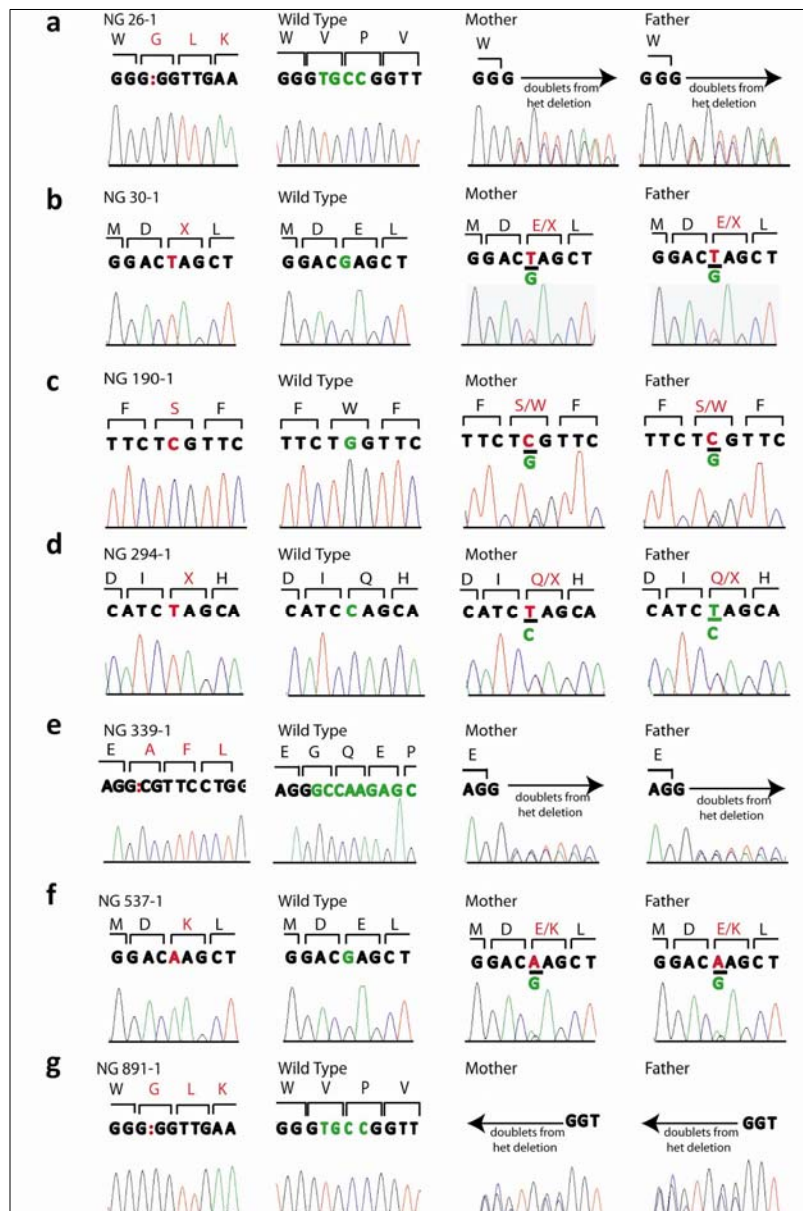
Supplementary Videos 5 and 6, Videos constructed from T1 sagittal (Supplementary Video 5) and coronal (Supplementary Video 6) images (photographically inverted) of patient NG 891-1 demonstrate radiographic findings consistent with microlissencephaly including prominent microcephaly, the extreme simplification of the gyral-sulcal pattern, markedly thickened cortex throughout and indistinct gray-white junction. There are bilateral Sylvian clefts, and the corpus callosum is hypoplastic.

Supplementary Figures

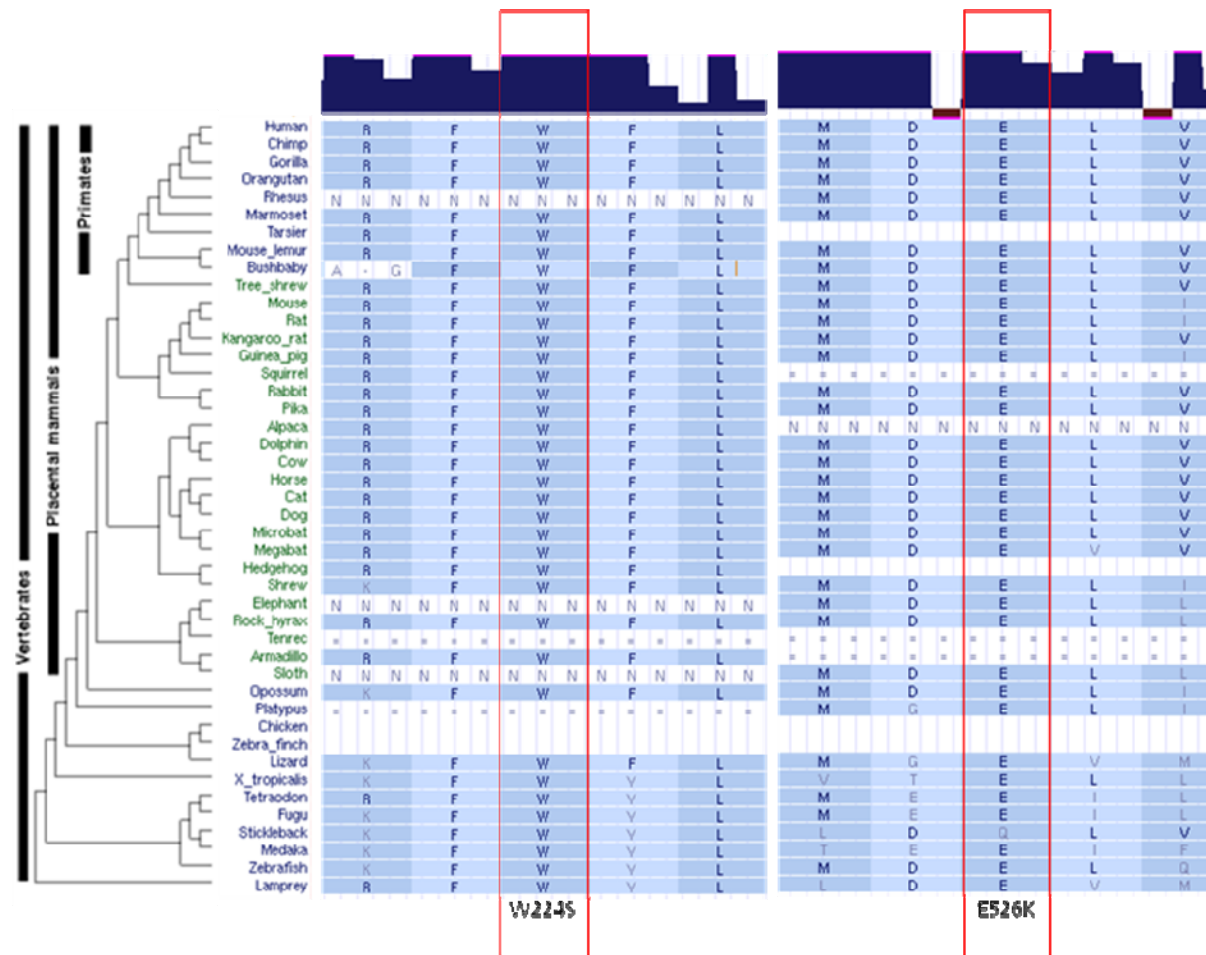


Supplementary Fig. 1 | Two novel homozygous missense variants identified within the shared homozygosity regions of affected individuals of family NG 26. Left panel: On chromosome 12, position 130,807,115, an A to G transition results in a Thr to Ala substitution in the non-conserved 565th residue (marked with the red box) of *Splicing Factor, Arginine/Serine-rich 8* (*SFRS8*).

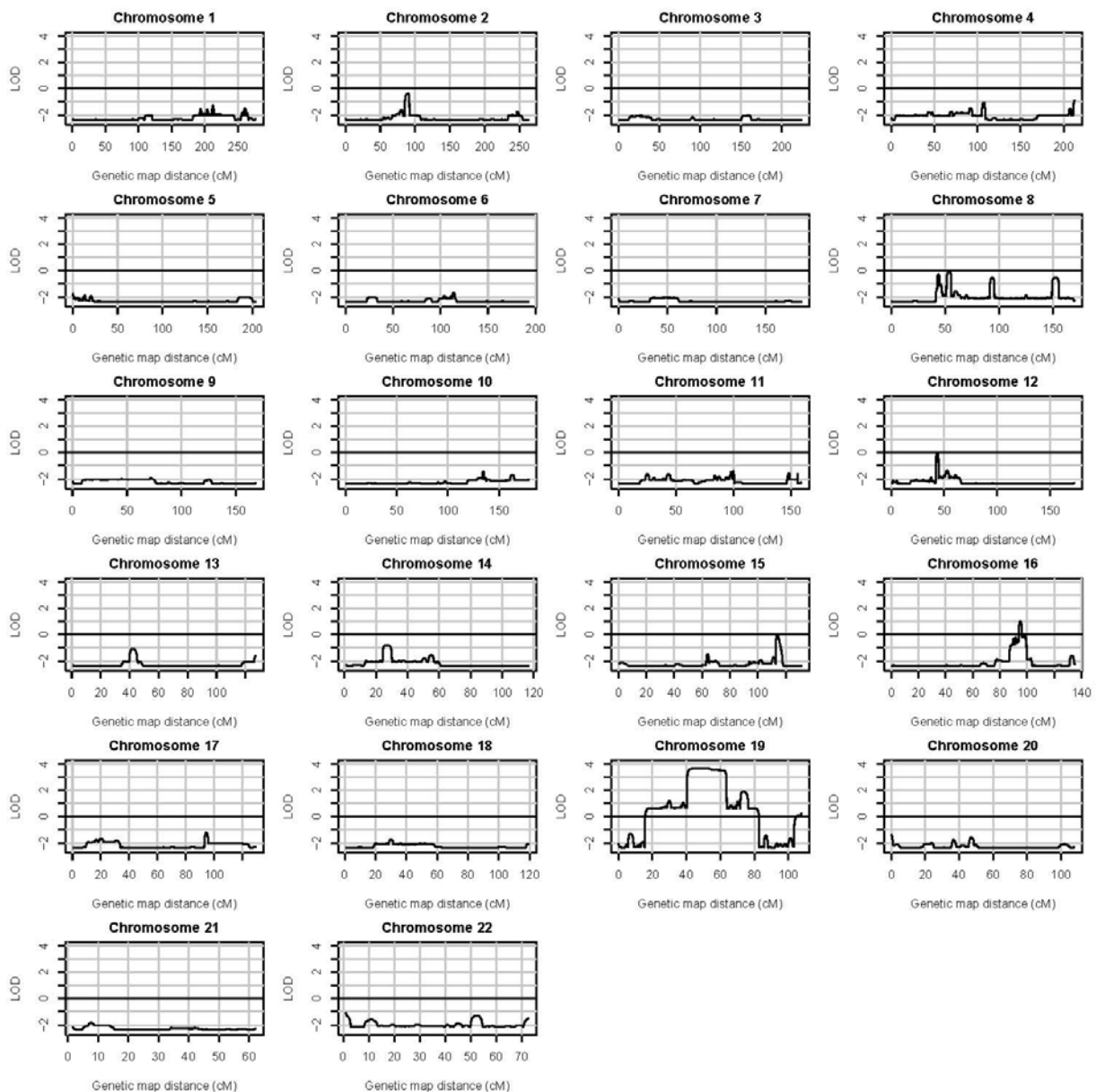
Right panel: Similarly, in *IBTK* (*Inhibitor of Bruton Agammaglobulinemia Tyrosine Kinase*), a G to C substitution on chromosome 6, position 82,980,721, results in a Pro to Ala substitution of the 716th residue of the protein (red box) which is not highly conserved across 44 vertebrate species (from <http://www.genome.ucsc.edu>: Kent WJ, et al. The human genome browser at UCSC. Genome Res. 2002 Jun;12(6):996-1006.)



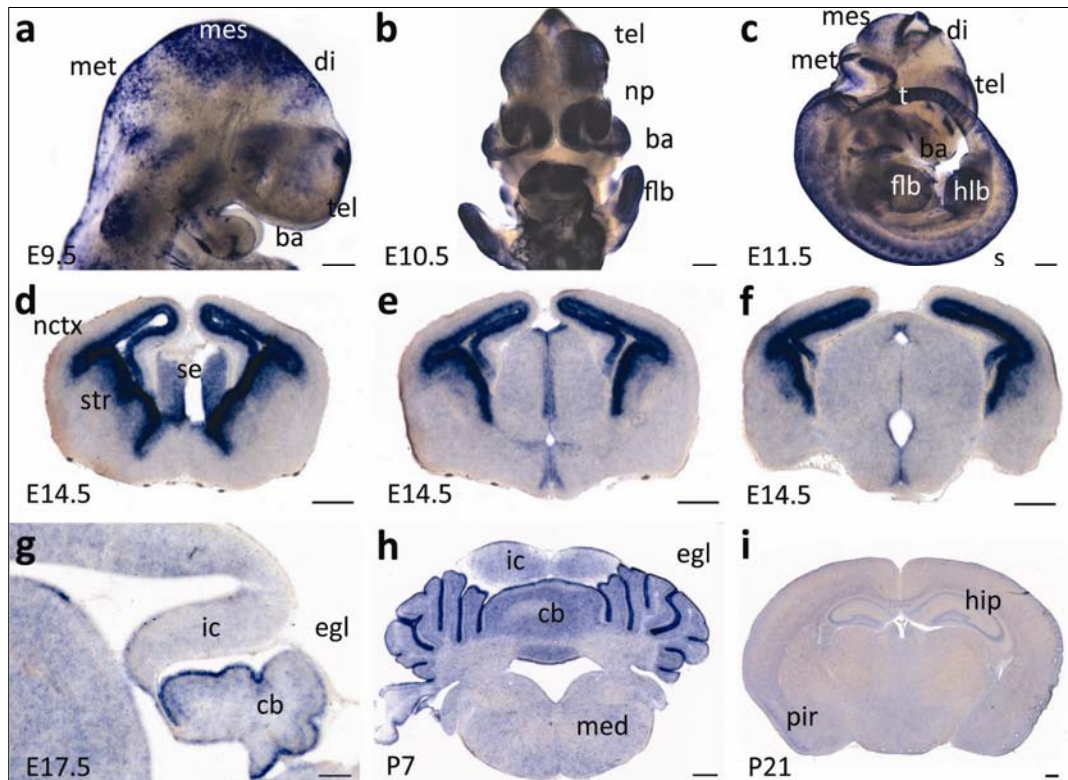
Supplementary Fig. 2 | Sequence traces of 7 families with *WDR62* mutations. From left to right, the panels show the DNA sequences of the patients, control subjects, and the patients' parents, respectively. The predicted amino acids corresponding to each codon are represented above the nucleotide sequences, which are marked in bold letters above the chromatograms. For each sequence, the mutated base(s) are shown in red, as are resultant amino acid substitutions. For the wild type sequences, the altered bases are shown in green. Note that all patients are homozygous for the mutations while both parents are heterozygous. The following mutations are observed: (a) NG 26: V1402GfsX12, (b) NG 30: E526X, (c) NG 190: W224S, (d) NG 294: Q470X, (e) NG 339: G1280AfsX21, (f) NG 537: E526K, (g) NG 891: V1402GfsX12.



Supplementary Fig. 3 | Sequence alignment of vertebrate WDR62 proteins. Missense mutations identified in NG 190 (W224S) and NG 537 (E526K) alter two highly conserved amino acid residues across 44 vertebrates (with the exception of Stickleback for position 526). (from <http://www.genome.ucsc.edu>: Kent WJ, et al. The human genome browser at UCSC. Genome Res. 2002 Jun;12(6):996-1006.)

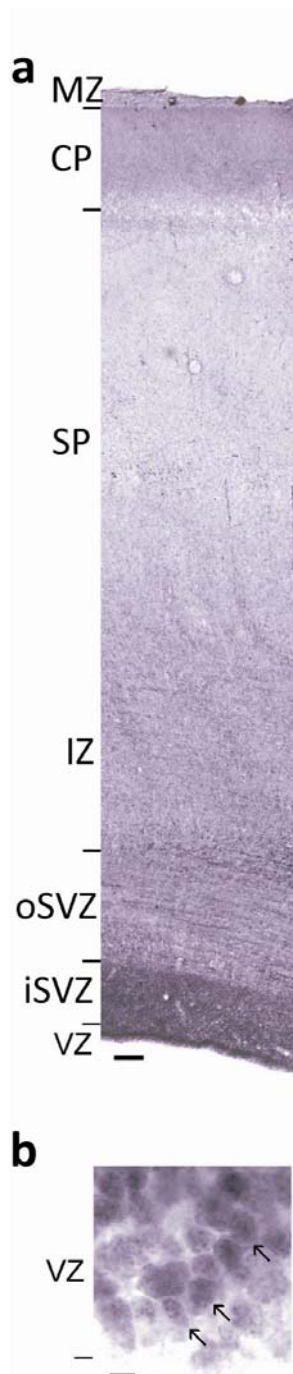


Supplementary Fig. 4 | Genome-wide linkage analysis of pedigree NG 190 with three affected and one unaffected family members. For linkage analysis, an autosomal recessive mode of inheritance with a phenocopy rate of 0.001, penetrance rates of 0.001 and 0.99 for heterozygous and homozygous conditions, respectively, were assumed. Disease causing allele frequency was set to 0.001. The vertical axis corresponds to LOD score and the horizontal axis shows genetic distance in centimorgans (cM). The linkage graphs for all autosomal chromosomes are shown. The maximum LOD score for the chromosome 19 locus spanning the *WDR62* gene, located between 41,237,623 and 41,287,852 base pairs is 3.64. The LOD-3 interval is marked by markers rs3855681 and rs7359950, located at 16,259,314 (40.1 cM) and 44,455,605 (63.8 cM) base pairs, respectively.



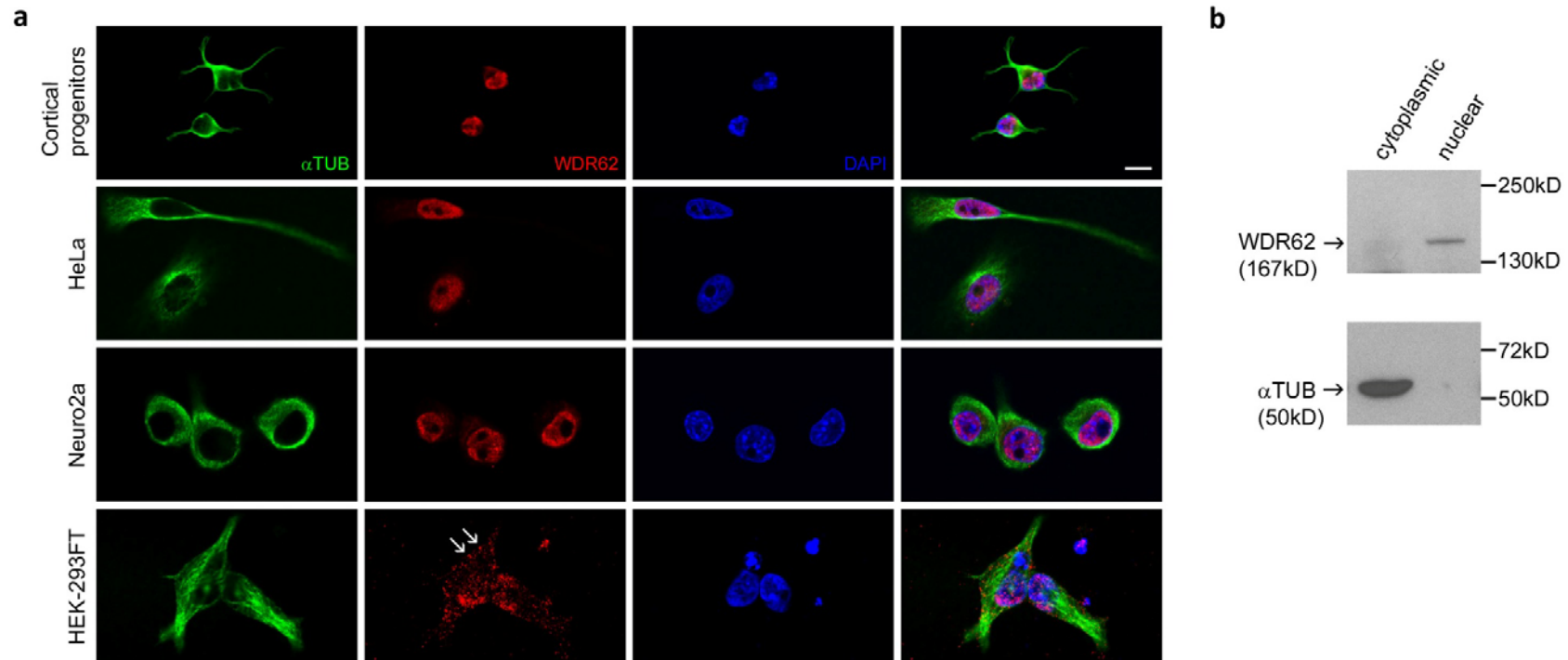
Supplementary Fig 5 | *Wdr62* expression in the developing mouse brain.

a-c, Whole mount in situ hybridization at E9.5 to E11.5. Lateral (panels a and c) and frontal views (panel b) are shown. *Wdr62* mRNA is detected in the telencephalon (tel), diencephalon (di), mesencephalon (mes), metencephalon (met), branchial arch (ba), nasal process (np), forelimb bud (flb), hindlimb bud (hlb), somites (s) and tail (t). d-f, Coronal sections of the developing forebrain at three different rostrocaudal levels at embryonic day 14.5 (E14.5) are shown. *Wdr62* expression is detected in proliferating neuronal progenitors in the neuroepithelium of the neocortex (nctx), striatum (str) and septum (se). g-h, Sagittal (g) and axial (h) sections of the cerebellum at E17.5 and postnatal day 7 (P7) mouse. *Wdr62* mRNA is detected in proliferating granule neuron precursors in the external granular layer (egl) of the developing cerebellum (cb). Expression is absent from the inferior colliculus (ic) and the medulla (med). i, Coronal section of the forebrain of P21 mouse. *Wdr62* mRNA expression is detected at low levels in the hippocampus (hip) and piriform cortex (pir). Scale bars: 0.2 mm (a, g to i), 0.5 mm (panels b to f).

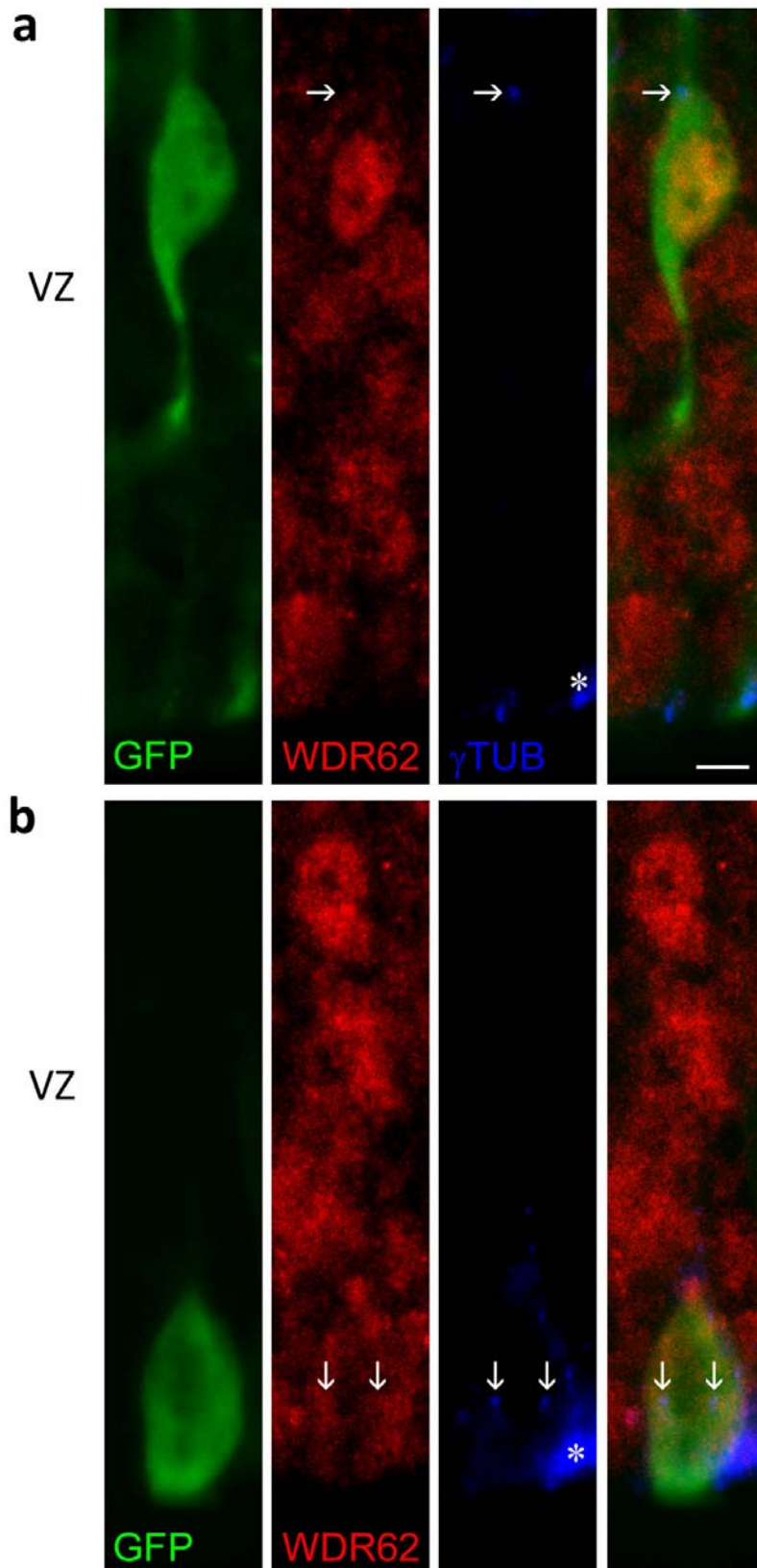
**Supplementary Fig 6 | WDR62 expression in the developing human brain.**

a, Immunohistochemical staining in 20 weeks of gestation human fetal neocortex: In the developing human brain, similar to the mouse brain, WDR62 is enriched in the ventricular and subventricular zones (VZ and SVZ, respectively) and weakly present in the cortical plate (CP) (scale bar: 200 μm). iVZ: inner ventricular zone; oSVZ: outer subventricular zone; IZ: intermediate zone; SP: subplate; MZ: marginal zone.

b, In VZ cells near the ventricular surface, WDR62 is localized to nuclei (arrows) (scale bar: 5 μm).



Supplementary Fig. 7 | a, Immunofluorescent staining for α -tubulin (green), WDR62 (red, using mouse anti-WDR62 (Sigma-Aldrich) antibody), and counterstaining by DAPI (blue) in cultured E12.5 mouse cortical neural progenitors, HeLa, Neuro2a, and HEK-293FT cells. WDR62 localization is nuclear in cortical neural progenitors, HeLa, and Neuro2a cells. In HEK-293FT cells, WDR62 is localized to granules (arrows) as previously described by Wasserman et al, 2010 (Mol Bio Cell, 21:117-130, 2010). Scale bar: 10 μ m. b, Subcellular fractionation of mouse E14.5 neocortex and immunoblotting for WDR62 (using rabbit anti-WDR62 antibody, Novus) reveal that WDR62 is present in the nuclear fraction.

**Supplementary Fig. 8 |**

Immunofluorescent staining of E15.5 mouse neocortex electroporated in utero with CAG-GFP at E13.5.

a, In a GFP-filled VZ cell positioned away from the ventricular surface, WDR62 localization is nuclear and does not overlap with the single centrosome (arrow) marked by γ -tubulin (blue). Radial glial endfoot staining of γ -tubulin is indicated (asterisk).

b, In a GFP-filled mitotic cell in metaphase at the ventricular surface, WDR62 is relocalized to the cytoplasm upon chromatin condensation and the breakdown of the nuclear membrane and does not apparently co-localize with the two centrosomes (arrows) marked by γ -tubulin.

Scale bar: 5 μ m in a, b.

Composite images are shown as the right most images.

Supplementary Tables

Supplementary Table 1 | Blocks of shared homozygosity between the two affected individuals of family NG 26

Chromosome	Start	End	SNP Start	SNP End	Number of SNPs	Length (cM)	Length (Mb)
1	240,862,637	247,177,330	rs10926796	rs6704311	623	10.90	6.31
6	82,149,868	87,794,412	rs2120536	rs7740936	510	2.96	5.64
12	125,564,137	132,288,869	rs16920745	rs7975069	907	20.79	6.72
19	8,931,837	14,582,019	rs2547067	rs6511944	510	9.16	5.65
19	36,896,151	47,035,366	rs10417470	rs3922888	894	13.17	10.14
X	147,386,161	154,582,606	rs5980537	rs557132	478	23.13	7.20
Total					3,922	80.11	41.66

Supplementary Table 2 | Coverage distribution across the exome*

Read Length	Number of lanes	Read Type	Number of Reads	Reads Mapped to the Genome	Reads Mapped to the Exome	Average Coverage Across The Exome	Bases Covered \geq 4X within the Exome
74	2	Single end	37.1M	97.3%	57.40%	44.3X	94.34%

* In two lanes of single-end 74 base pair reads, we obtained 37 million reads, 21 million of which mapped to the exome, and 466,000 of which mapped to the 969,174 exomic base pairs (out of 41.66 million genomic base pairs) in shared regions of homozygosity between the two affected siblings (Supplementary Table 1). The sequence error rate (per base per read) was 0.34%. Sensitivity and specificity for detection of homozygous variation from the reference sequence was high (both >97%) as determined by comparison of the sequencing data to the results of SNP genotyping as a reference.

Supplementary Table 3 | Novel missense variants and insertion/deletions leading to a frame-shift mutation in NG 26-1

Chr	Position	Base change	Quality Score	Coverage	Major allele (no PCR duplicates)	Minor allele (no PCR duplicates)	Gene	Status	Amino acid change	Amino acid position
6	82,980,721	G to C	228	43	11	5	IBTK	Missense	P716A	716/1353
12	130,807,115	A to G	96	20	7	0	SFRS8	Missense	T565A	565/951
19	41,287,310	-TGCC deletion	163/391	6	4	0	WDR62	Frame-shift	V1402GfsX12	1402/1523

Supplementary Table 4 | Four potential heterozygous missense variants identified in a total of 100 exome sequencing experiments of subjects without neurological diseases

Sample ID	Chr	Position	Base Change	Amino Acid Change	Amino Acid Location
RKH005	chr19	41,284,406	A>T	D991V	991/1523
PTH120	chr19	41,285,904	G>A	A1152T	1157/1523
PTH108	chr19	41,284,409	C>T	S992L	992/1523
LMB06	chr19	41,285,506	T>C	V1083A	1083/1523

Supplementary Table 5 | Radiographic characteristics of patients with *WDR62* mutations

Patient ID	Cortical Thickening	Microcephaly	Pachygyria	Polymicrogyria	Schizencephaly	Under-opercularization	Cerebellum	Hippocampus	Corpus Callosum	
									Rostrum	Splenium
NG 26-1	+	+	+	R temporal and RL occipito-parietal	-	+	Normal	Normal	Mild hypoplasia	Mild hypoplasia
NG 30-1	+	+	+	-	-	-	Normal	Dysmorphic	Absent	Moderate Hypoplasia
NG 190-1	+	+	+	L fronto-temporal-parietal	L parietal	+	Normal	Dysmorphic	Absent	Marked Hypoplasia
NG 190-5	+	+	+	-	-	-	R hypoplasia	Dysmorphic	Absent	Marked Hypoplasia
NG 190-6	+	+	+	-	-	-	Normal	Dysmorphic	Mild hypoplasia	Normal
NG 294-1	+	+	+	-	-	+	Normal	Dysmorphic	Mild hypoplasia	Marked Hypoplasia
NG 339-1	+	+	+	-	-	+	Normal	Dysmorphic	Absent	Marked Hypoplasia
NG 537-1	+	+	+	-	-	+	Normal	Normal	Mild hypoplasia	Normal
NG 891-1	+	+	+	-	-	+	Normal	Normal	Mild hypoplasia	Moderate Hypoplasia

R: right, L: left

Supplementary Table 6 | Representative genes linked to developmental brain malformations with expression patterns correlating with that of *Wdr62*

Symbol	<i>Wdr62</i> correlation	<i>P</i> value	Malformation	References
<i>Dcx</i>	-0.95	3.00E-08	X-linked lissencephaly-1; Double Cortex Syndrome	Cell 92: 51-61, 1998; Cell 92: 63-72, 1998
<i>Tuba1a</i>	-0.94	5.80E-08	Lissencephaly type 3	Cell 128: 45-57, 2007; Hum. Mutat. 28: 1055-1064, 2007
<i>Dcc</i>	-0.94	9.71E-08	Congenital Mirror Movements (Bimanual Synergia)	Science 328: 592-only, 2010
<i>Bub1b</i>	0.93	1.18E-07	Mosaic Variegated Aneuploidy Syndrome (MVA), microcephaly	Am. J. Med. Genet. 140A: 358-367, 2006
<i>Cc2d2a</i>	0.94	5.47E-08	Joubert Syndrome 9; Type 6 Meckel Syndrome	Am. J. Hum. Genet. 82: 1011-1018, 2008; Am. J. Hum. Genet. 82: 1361-1367, 2008
<i>Col18a1</i>	0.95	2.36E-08	Type 1 Knobloch Syndrome	Hum. Molec. Genet. 9: 2051-2058, 2000; Hum. Mutat. 23: 77-84, 2004